Optics Letters

Long-range multicore optical fiber displacement sensor

Monserrat C. Alonso-Murias,[1] David Monzón-Hernández,[1,*] Osvaldo Rodríguez-Quiroz,[1] J. Enrique Antonio-Lopez,[2] Axel Schülzgen,[2] Rodrigo Amezcua-Correa,[2] and Joel Villatoro[3,4]

[1]Centro de Investigaciones en Óptica A. C., Loma del Bosque 115 C. P. 37150, León, Guanajuato, Mexico
[2]CREOL The College of Optics and Photonics, University of Central Florida, Orlando, Florida 162700, USA
[3]Department of Communications Engineering, University of the Basque Country UPV/EHU, Bilbao, 48013, Spain
[4]IKERBASQUE-Basque Foundation for Science, Bilbao E-48011, Spain
*Corresponding author: dmonzon@cio.mx

Received 10 February 2021; revised 16 March 2021; accepted 8 April 2021; posted 9 April 2021 (Doc. ID 421004); published 30 April 2021

In this Letter, a long-range optical fiber displacement sensor based on an extrinsic Fabry–Perot interferometer (EFPI) built with a strongly coupled multicore fiber (SCMCF) is proposed and demonstrated. To fabricate the device, 9.2 mm of SCMCF was spliced to a conventional single-mode fiber (SMF). The sensor reflection spectrum is affected by super-mode interference in the SCMCF and the interference produced by the EFPI. Displacement of the SMF-SCMCF tip with respect to a reflecting surface produces quantifiable changes in the amplitude and period of the interference pattern in the reflection spectrum. Since the multicore fiber is an efficient light collecting area, sufficient signal intensity can be obtained for displacements of several centimeters. By analyzing the interference pattern in the Fourier domain, it was possible to measure displacements up to 50 mm with a resolution of approximately 500 nm. To our knowledge, this is the first time that a multicore fiber has been used to build a displacement sensor. The dynamic measurement range is at least seven times larger than that achieved with an EFPI built with a conventional SMF. Moreover, the SMF-SCMCF tip is robust and easy to fabricate and replicate.

https://doi.org/10.1364/OL.421004

Interferometry is a powerful optical technique that has contributed to the development of several fields of modern science and technology [1]. Interferometers have been continuously evolving and adapting to take advantage of new technologies. In this regard, optical fiber interferometric sensors (OFISs) [2–4] represent a good example of a successful combination of interferometry and fiber optics [5–8]. Optical fiber interferometers are appealing for sensing applications since they combine the high sensitivity of interference with the versatility of optical fibers.

The rapid evolution that OFISs have experiences in the last few years is owed, in part, to the continuous evolution of fiber optics technology. For example, new OFISs can be fabricated with novel specialty optical fibers (SOFs). The advent of a particular SOF, namely, strongly coupled multicore fiber (SCMCF), has opened up new alternatives to develop sensitive and versatile OFISs [9–14].

In the majority of SCMCF interferometers, the sensing mechanism is based on changes in the physical length of the SCMCF or on changes in the refractive index of the cores. Interferometers based on SCMCF have been demonstrated for the development of compact, robust, highly stable, and highly sensitive sensors for real-time monitoring of physical magnitudes such as temperature, bending, vibration, strain, and torsion, among others [9–16]. In all the interferometers based on SCMCFs proposed so far, shifts in the transmitted or reflected spectrum are monitored and correlated with the parameter being sensed.

The cross-section of an SCMCF and the unique field distribution of the super-modes have not been exploited yet. Thus, in this Letter, an extrinsic Fabry–Perot interferometer (EFPI)-based long-range displacement sensor using a seven-core SCMCF is demonstrated. To do so, a few millimeters of such an SCMCF were spliced at the distal end of an SMF. Due to the presence of multiple identical cores around the central core in the SCMCF, the light collecting area, in comparison with that of an SMF, is significantly increased. This feature allows to measure displacements up to 50 mm with a resolution of 500 nm, approximately. The analysis of the reflection spectrum of the sensor proposed here, which is composed of a pair of superposed interference patterns, was carried out in the Fourier domain.

The cross-section of the SCMCF used in this work is depicted in Fig. 1(a). The fiber consists of a central core with six surrounding cores. Each core has a diameter of 9 μm. The distance from center to center of adjacent cores is 11 μm. The numerical aperture of each core at 1550 nm is 0.14. The cores are made of germanium doped silica glass, and the surrounding cladding is made of pure silica glass. The SCMCF was fabricated by the stack and draw method at the University of Central Florida.

To measure displacements, the structure shown in Fig. 1(a) was fabricated and placed in front of a reflecting surface, as shown in Fig. 1(b). To construct the fiber tip shown in Fig. 1(a), a segment of SCMCF was spliced to an SMF by using a default

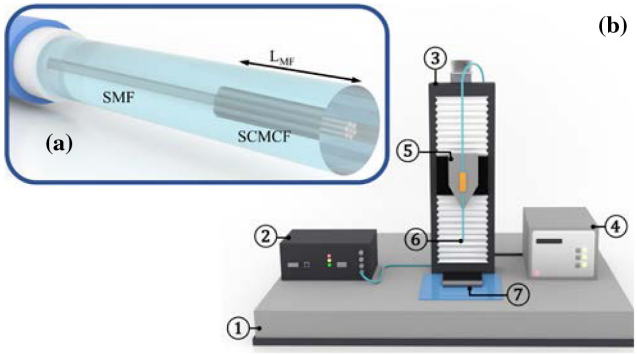

Fig. 1. (a) Representation of fiber tip structure. (b) Experimental setup: 1. optical table, 2. FBG interrogator, 3. motorized translation stage, 4. stepper motor controller, 5. V-groove fiber holder, 6. fiber tip, and 7. mirror.

fusion splicing program set up in a splicer, model FSM-100P (Fujikura). Then the SCMCF was cleaved to a length (L_{MF}) previously calculated.

It is well known that in an SMF-SCMCF structure, with axial symmetry, two super-modes are excited in the multicore fiber [17,18]. These super-modes with different propagation constants, denoted as β_1 and β_2, propagate through the SCMCF and are reflected from the cleaved SCMCF end. The accumulated phase difference between the super-modes after propagating and reflecting from the SCMCF end is $\Delta\phi = 2(\beta_1 - \beta_2)L_{MF}$. The interference of the two excited super-modes is responsible for the modulation in the reflection spectrum of an SMF-SCMCF structure [12,14,16,19].

Approximately 4% of the incident light intensity is reflected from the cleaved SCMCF end. Therefore, when a reflective surface is placed in front of and parallel to the SCMCF tip end-face an EFPI is formed. Light exiting from the cores of the SCMCF propagates through the air gap until it is reflected by the mirrored surface. A portion of that light is recoupled into the SCMCF. The superposition of the internally reflected super-modes and the beam reflected from the external surface gives rise to interference, which is combined with the super-mode interference.

To elucidate the role of the length of the SCMCF in the interference of the EFPI, and hence on the performance of the displacement sensor, the field distribution at the end-face of the SCMCF was simulated using commercial software (MODE from Lumerical). The beam propagation, at 1550 nm, in SMF-SCMCF structures with L_{MFs} of 5.2 and 9.2 mm, is shown in Figs. 2(a) and 2(c). In both cases, periodic transfer of energy from the central core to the neighbor cores happens at a distance known as coupling length (L_c), which is given as $L_c = \pi/(|\beta_2 - \beta_1|)$. The beam profiles for these two values of L_{MF} are shown in Figs. 2(b) and 2(d).

At the end of the SCMCF, the light is in the central core due to constructive super-mode interference, which occurs when $L_{MF} = mL_c$, with m an integer number. The light will be in the cores surrounding the central core when $L_{MF} = (2m + 1)L_c/2$. These two cases, shown in Figs. 2(b) and 2(d), represent two distinctive possibilities to measure distance that will be discussed below.

Thus, two SMF-SCMCF tips, one with an L_{MF} of 5.2 ± 0.2 mm and the other with 9.2 ± 0.2 mm, were fabricated. The reflected spectra of the SMF-SCMCF tips are

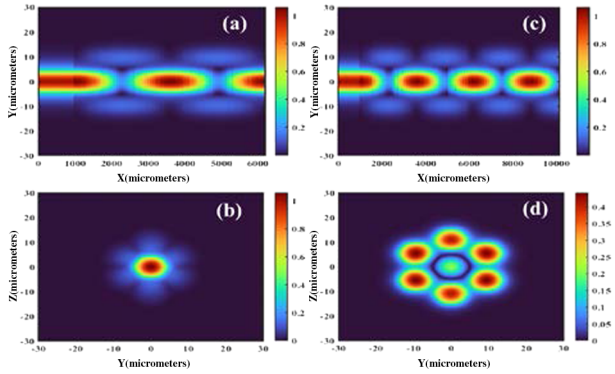

Fig. 2. Transversal view of light propagation along the SCMCF when L_{MF} is equal to (a) 5.2 mm and (c) 9.2 mm at 1550 nm. Mode distribution at the fiber end-face of the SCMCF when L_{MF} is equal to (b) 5.2 mm and (d) 9.2 mm at 1550 nm.

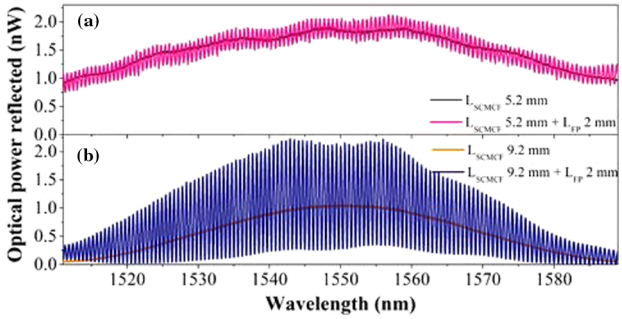

Fig. 3. (a) Reflection spectrum of the SCMCF interferometer (black line) and SCMCF interferometer + EFPI interferometer (pink line). L_{MF} is 5.2 mm. (b) Reflection spectrum of the SCMCF interferometer (orange line) and SCMCF interferometer + EFPI interferometer (navy line). L_{MF} is 9.2 mm. In both cases, the air cavity length of EFPI is 2 mm and a seven-core SCMCF is used.

shown with a black line in Fig. 3(a) and orange line in Fig. 3(b). As can be seen, in both interference spectra, there is just one maximum in the wavelength span, and this maximum occurs ca. 1550 nm. These characteristics are determined by L_{MF}. The spectra shown in Fig. 3 were obtained by connecting the free end of the SMF to a fiber Bragg grating (FBG) interrogator, model si125 from Micron Optics.

To measure displacements, the SMF-SCMCF tips were fixed on a V-groove holder that was on a motorized translation stage (NRT150/M, from Thorlabs), as shown in Fig. 1(b). The distance (L_{FP}) between the SMF-SCMCF tip and the reflecting surface was initially set to zero, i.e., the SMF-SCMCF tip was touching the surface. Then the tip was gradually separated from this surface. The reflection spectra observed with the samples of L_{MF} of 5.2 and 9.2 mm, and an $L_{FP} = 2$ mm, are shown in Figs. 3(a) and 3(b). The period of the modulation is very similar in both cases, but the difference in the amplitude of the interference patterns is evident. The interference pattern in Fig. 3(a) is quite similar to that obtained when an EFPI is constructed with an SMF tip that can be used to measure displacements shorter than 10 mm [20].

The reason for the differences between the spectra shown in Figs. 3(a) and 3(b) is how the light exits from the end-face of the SCMCF [Figs. 2(b) and 2(d)]. If the beam that exists from the

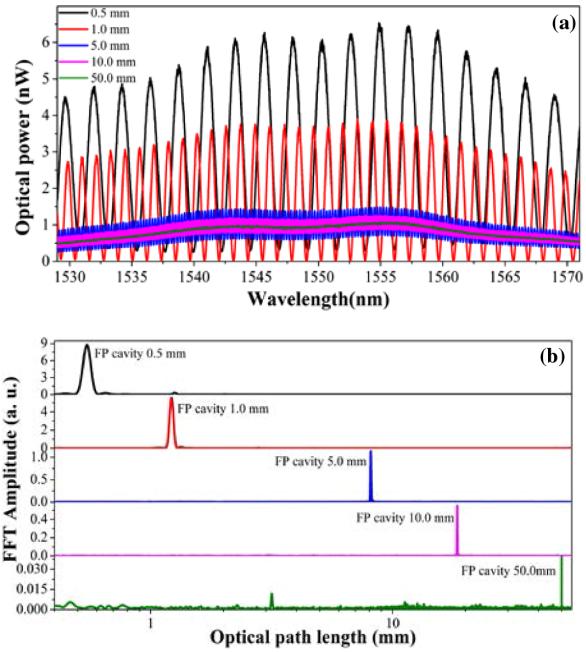

Fig. 4. Reflection spectra of the EFPI with different air cavity lengths in (a) optical and (b) Fourier domains; the optical path length axis is in logarithmic scale.

SCMCF is broad, it diffracts more slowly, and the measuring range is enlarged. By comparing the spectra obtained with the two fabricated SMF-SCMCF tips, it is evident that the tip with $L_{MF} = 9.2$ mm is better for distance sensing applications.

Thus, the tip fabricated with 9.2 mm of SCMCF was fixed to a V-groove holder of the experimental setup represented in Fig. 1(b). The translation stage was moved to put the fiber tip in direct contact with the mirror located over the optical table. The fiber tip was then displaced from the initial position to a distance of 20 mm in steps of 0.1 mm, and then from 20 mm to 50 mm with steps of 1 mm. At each step, the reflection spectrum was recorded, and the corresponding Fourier spectrum was calculated.

The reflection spectra when the SMF-SCMCF tip was located at 0.5, 1.0, 5.0, 10.0, and 50.0 mm from the mirror are shown in Fig. 4(a). It can be seen that fringe contrast decreases drastically when the fiber tip is far from the mirror. The Fourier transforms of the spectra shown in Fig. 4(a) were calculated by using a MATLAB code of the algorithm described in Ref. [21]. The results are shown in Fig. 4(b). Each peak shown in Fig. 4(b) corresponds to the interference produced by the EFPI air cavity, and the position of the peak in the x axis (optical path length) corresponds to the distance of the SMF-SCMCF tip from the mirror. The label of each graph describes the total displacement, or L_{FP}, of the mechanical translation stage from the initial position. The uncertainty to determine the exact position of the maximum of the peak produced an error of around 200 nm. This error is larger for air cavities longer than 20 mm due to the small amplitude of the Fourier peak produced by the small fringe visibility of the interference pattern.

The amplitude of the FFT peak as a function of the separation of the SMF tip and SMF-SCMCF tip from the mirror is shown in Fig. 5. The peak with the highest amplitude, which it is related directly to the fringe visibility, occurred for $L_{FP} = 0.30$ mm. For comparison, the peak with the highest amplitude, in

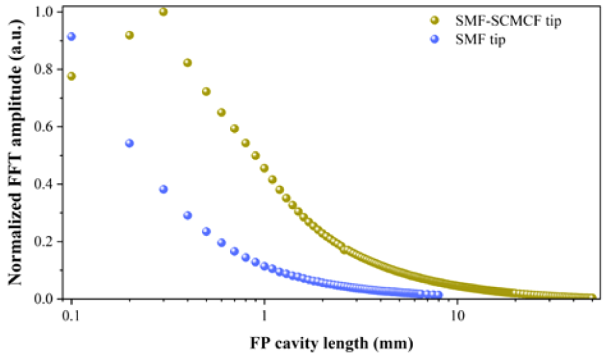

Fig. 5. Behavior of the amplitude of the peak of Fourier spectra calculated from optical reflection spectra produced by the EFPI based on the SMF-SCMCF tip (yellow sphere) and the SMF tip (blue sphere). The FP cavity length axis is in logarithmic scale.

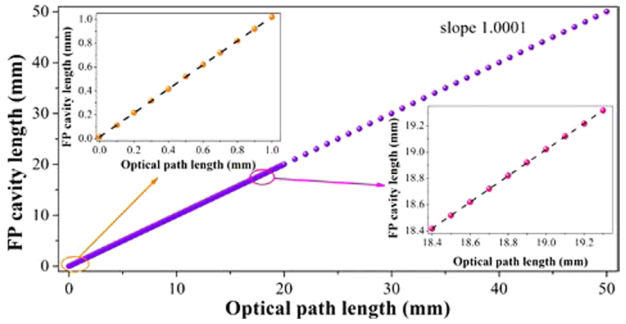

Fig. 6. Measured optical path length with EFPI interferometers as a function of input Fabry–Perot air cavity.

an EFPI using a SMF tip, occurs for an air cavity length of 0.05 mm.

In Fig. 6, the optical path length calculated from the Fourier spectra versus Fabry–Perot cavity length achieved by the displacement of the mechanical mount where the fiber tip was attached is shown. There is a very good agreement between the displacement of the SMF-SCMCF tip with the translation stage and the displacement calculated from the optical interference spectra. In the inset graphs, a close-up of the curve is shown at the fiber displacement close to zero and when the fiber displacement was close to 20 mm.

It is important to point out that several methods have been proposed so far to increase the displacement range of an EFPI, for example, by splicing a micrometric section of graded-index multimode fiber to the end of an SMF [22], by attaching a bulky collimator at the end of an SMF [23], or by using a tapered SMF tip [24]. However, these methods are complicated and difficult to replicate and require specialized equipment and trained experts. The fiber tip proposed here involves splicing only a short segment of SCMCF with a conventional SMF and cleaving the multicore fiber to a proper length. Commercially available fiber cleavers ensure a cleaving angle of less than 0.2°. Similar angles can be achieved if the SCMCF tip is polished. Thus, SCMCFs with flat ends can be fabricated with widely available tools and machines.

One important aspect in the performance of any sensor is the resolution that can be achieved. To determine the measurement resolution of the displacement sensor proposed in this work, the SMF-SCMCF tip was attached to a Nano-max-TS from

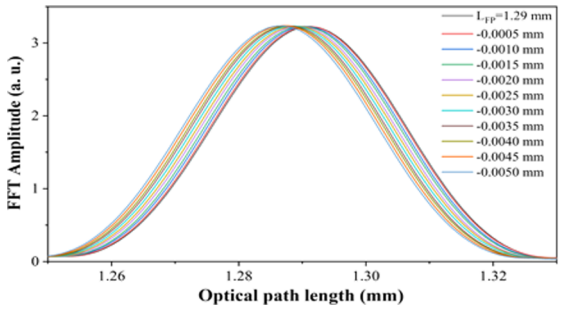

Fig. 7. Reflection spectra of the EFPI with different air cavity lengths in the Fourier domain.

Thorlabs, and the fiber tip was placed at 1.29 mm from the mirror. Then, the tip was moved in steps of 500 nm towards the mirror with the motorized translation stage. At each position, the optical spectrum of the reflection signal was recorded. A close-up of the calculated Fourier spectra is shown in Fig. 7. It can be seen that it is possible to distinguish the changes in the peak position when the fiber tip is displaced by 500 nm. The procedure to determine the maximum of the peak in the Fourier spectrum can be automatized to improve the resolution. Conversely, if the objective is to achieve a sub-nanometer resolution, there are a number of algorithms [25–27] proposed so far that can be implemented.

In conclusion, in this Letter, an extrinsic multicore fiber Fabry–Perot long-range displacement sensor was proposed and demonstrated. A 9.2 mm long section of seven-core fiber was used to fabricate an SMF-SCMCF tip. At such a length, the super-modes interfere destructively in the central core and constructively in the surrounding cores. Thus, the light that exits from the SMF-SCMCF tip is broad and suffers less diffraction. All this contributes to increasing the displacement range measurement. Here, we have demonstrated the measuring of displacement up to 50 mm with nanometer resolution. The advantages of our device include straightforward and repeatable fabrication, low cost, and compactness. We believe that the EFPI displacement sensor proposed here can be useful for many real-world applications in which nanometric or micrometric displacements occur, for example, due to vibrations, pressure, or force.

Funding. Spain Ministerio de Ciencia, Innovación y Universidades (PGC2018-101997-B-I00); Mexico Consejo Nacional de Ciencia y Tecnología.

Disclosures. The authors declare no conflicts of interest.

Data Availability. Data underlying the results presented in this paper are not publicly available at this time but may be obtained from the authors upon reasonable request.

REFERENCES

1. P. Hariharan, *Optical Interferometry*, 2nd ed. (Academic, 2003).
2. V. Vali and R. W. Shorthill, Appl. Opt. **15**, 1099 (1976).
3. S. K. Sheem and T. G. Giallorenzi, Appl. Phys. Let. **35**, 914 (1979).
4. D. A. Jackson, A. Dandridge, and S. K. Sheem, Opt. Let. **5**, 139 (1980).
5. H. C. Lefèvre, Opt. Fiber Technol. **19**, 828 (2013).
6. J. A. Bucaro and H. D. Dardy, J. Acoust. Soc. Am. **62**, 1302 (1977).
7. A. Dandridge, Opt. Photon. News **30**(6), 34 (2019).
8. Y. N. Korkishko, Y. N. Korkishko, V. A. Fedorov, V. E. Prilutskii, V. G. Ponomarev, I. V. Morev, S. M. Kostritskii, A. I. Zuev, and V. K. Varnakov, Proc. SPIE **8421**, 842107 (2012).
9. J. E. Antonio-Lopez, Z. S. Eznaveh, P. LiKamWa, A. Schülzgen, and R. Amezcua-Correa, Opt. Lett. **39**, 4309 (2014).
10. R. Amezcua-Correa, A. Schulzgen, and J. E. Antonio-Lopez, "Multicore optical fiber apparatus, methods, and applications," U.S. patent WO2015163963A2 (17 December 2015).
11. J. Villatoro, A. Van Newkirk, E. Antonio-Lopez, A. Schülzgen, and R. Amezcua-Correa, Opt. Lett. **41**, 832 (2016).
12. J. Villatoro, E. Antonio-Lopez, A. Schülzgen, and R. Amezcua-Correa, Opt. Lett. **42**, 2022(2017).
13. J. Villatoro, O. Arrizabalaga, G. Durana, I. Saéz de Ocáriz, E. Antonio-Lopez, J. Zubia, A. Schülzgen, and R. Amezcua-Correa, Sci. Rep. **7**, 4451 (2017).
14. J. Villatoro, E. Antonio-Lopez, A. Schülzgen, and R. Amezcua-Correa, Opt. Express **25**, 25734 (2017).
15. F. Tan, Z. Liu, J. Tu, C. Yu, C. Lu, and H.-Y. Tam, Opt. Express **26**, 19835 (2018).
16. Z. Liu, D. Zheng, J. Madrigal, J. Villatoro, E. Antonio-Lopez, A. Schülzgen, R. Amezcua-Correa, X. Zou, W. Pan, and S. Sales, Opt. Fiber Technol. **58**, 102315 (2020).
17. C. Xia, N. Bai, I. Ozdur, X. Zhou, and G. Li, Opt. Express **19**, 16653 (2011).
18. C. Xia, M. A. Eftekhar, R. Amezcua-Correa, J. E. Antonio-Lopez, A. Schülzgen, D. Christodoulides, and G. Li, IEEE J. Sel. Top. Quantum Electron. **22**, 196 (2016).
19. J. Amorebieta, G. Durana, A. Ortega-Gomez, R. Fernández, J. Velasco, I. Sáez de Ocáriz, J. Zubia, J. E. Antonio-López, A. Schülzgen, R. Amezcua-Correa, and J. Villatoro, J. Lightwave Technol. **37**, 2328 (2019).
20. K. A. Murphy, M. F. Gunther, A. M. Vengsakar, and R. O. Clauss, Opt. Lett. **16**, 273 (1991).
21. O. Rodriguez-Quiroz, C. E. Domínguez-Flores, D. Monzón-Hernández, and C. Moreno-Hernández, J. Lightwave Technol. **37**, 4268 (2019).
22. Y. Zhang, Y. Li, T. Wei, X. Lan, Y. Huang, G. Chen, and H. Xiao, IEEE Photon. J. **2**, 469 (2010).
23. K. T. Thurner, P. F. Braun, and K. Karrai, Rev. Sci. Instrum. **84**, 095005 (2013).
24. J. C. Moreno-Hernández, D. Monzón-Hernández, A. Martínez Ríos, D. Moreno-Hernández, and J. Villatoro, IEEE Photon. Technol. Lett. **27**, 379 (2015).
25. X. Zhou and Q. Yu, IEEE Sens. J. **11**, 1602 (2011).
26. H. C. Seat, P. Chawah, M. Cattoen, A. Sourice, G. Plantier, F. Boudin, J. Chéry, C. Brunet, P. Bernard, and M. Suleiman, Opt. Let. **37**, 2886 (2012).
27. N. Ushakov and L. Liokumovich, Appl. Opt. **53**, 5092 (2014).